

**Special Collection:**

The Frontiers in Jupiter Science and Exploration

**Key Points:**

- High-resolution simulations indicate that Jupiter's Alfvén radius is dynamic, exhibiting variations within a Jovian rotation period
- When averaged over a Jovian rotation period, the Alfvén radius's position aligns with the depiction of the static model
- The study underscores the need to integrate both short-term dynamics and long-term averages in understanding giant planetary magnetospheres

**Supporting Information:**

Supporting Information may be found in the online version of this article.

**Correspondence to:**Z. Yao,  
z.yao@ucl.ac.uk**Citation:**

Xu, Y., Ray, L., Yao, Z., Zhang, B., Bonfond, B., Badman, S., et al. (2024). Revealing the local time structure of the Alfvén radius in Jupiter's magnetosphere through high-resolution simulations. *Journal of Geophysical Research: Planets*, 129, e2024JE008368. <https://doi.org/10.1029/2024JE008368>


Received 29 FEB 2024

Accepted 28 MAY 2024

© 2024. The Author(s).

This is an open access article under the terms of the [Creative Commons Attribution License](#), which permits use, distribution and reproduction in any medium, provided the original work is properly cited.

## Revealing the Local Time Structure of the Alfvén Radius in Jupiter's Magnetosphere Through High-Resolution Simulations

Yan Xu<sup>1,2,3</sup> , Licia Ray<sup>3</sup> , Zhonghua Yao<sup>1,2,4,5</sup> , Binzheng Zhang<sup>5</sup> , Bertrand Bonfond<sup>6</sup> , Sarah Badman<sup>3</sup> , Denis Grodent<sup>6</sup> , Enhao Feng<sup>5</sup> , Tianshu Qin<sup>5</sup>, and Yong Wei<sup>1,2</sup>

<sup>1</sup>Key Laboratory of Earth and Planetary Physics, Institute of Geology and Geophysics, Chinese Academy of Sciences, Beijing, China, <sup>2</sup>College of Earth and Planetary Sciences, University of Chinese Academy of Sciences, Beijing, China, <sup>3</sup>Department of Physics, Lancaster University, Lancaster, UK, <sup>4</sup>Department of Physics and Astronomy, University College London, London, UK, <sup>5</sup>NWU-HKU Joint Centre of Earth and Planetary Sciences, Department of Earth Sciences, The University of Hong Kong, Hong Kong SAR, China, <sup>6</sup>Laboratoire de Physique Atmosphérique et Planétaire, STAR Institute, Université de Liège, Liège, Belgium

**Abstract** In the context of planetary magnetospheres, the Alfvén radius plays a critical role as the demarcation line where the planet's magnetosphere and ionosphere effectively decouple. This boundary is pivotal in understanding the complex interactions between planetary magnetic fields and space plasma environments. This study presents a dynamic analysis of the Alfvén radius within Jupiter's magnetosphere using high-resolution simulations to capture its temporal variability. Our simulations reveal that the Alfvén radius presents a dynamic behavior, which is strongly modulated by planetary rotation. However, when averaged over one Jovian rotation period, the location of the Alfvén radius displays striking similarities to that described by the statistical models proposed by Jenkins et al. (2024, [10.17635/lancaster/researchdata/661](https://doi.org/10.17635/lancaster/researchdata/661)). Specifically, our averaged results highlight a prominent outward bulge in the radius location toward ~03 local time with a notable absence of the radius between the noon and dusk sectors. The absence of the Alfvén radius suggests the higher Alfvén velocities in the noon-to-dusk sector associated with strong magnetic fields. These results suggest that while short-term dynamics are present, the average position of the Alfvén radius over a rotation period roughly remains consistent with previous steady-state models, providing an enhanced understanding of the long-term behavior exhibited by the magnetospheric plasma environment in Jupiter's magnetosphere. Importantly, the dynamic location of the Alfvén radius and the observed asymmetry after averaging over one rotation period could demonstrate a significant correlation with the complex evolution of the auroral enhancement.

**Plain Language Summary** In the vastness of space around Jupiter, there is an invisible boundary known as the Alfvén radius. It is an edge of Jupiter's magnetic influence where the planet's control over charged particles starts to wane. Inside this boundary, these particles are trapped and spin along with Jupiter as it rotates. Beyond the Alfvén radius, Jupiter's magnetic influence on the plasma will be greatly diminished. Our study investigates this boundary with high-resolution simulations, providing a more dynamic picture that captures its variation over time. Rather than a static feature, we show that the Alfvén radius is strongly affected by the rotation of the magnetosphere. When we average the boundary's position over one rotation period of Jupiter, it bears a striking resemblance to the static model proposed by Jenkins et al., including a bulge-like feature facing the night region and an absence of the boundary from noon to dusk. Our findings suggest that while Jupiter's magnetic environment is dynamic and fluctuating on short time scales, over longer periods, it shows a regularity that aligns with the static models. This work enhances our understanding of the long-term stability and structure of Jupiter's magnetosphere.

### 1. Introduction

The magnetosphere of Jupiter, the largest and most dynamic in our solar system, stands as a keystone in understanding planetary magnetic environments. This magnetosphere was significantly influenced by Io's plasma (e.g., Hill et al., 1983), extends outwards many Jovian radii ( $R_J$ ) from the planet, with a bi-modal distribution of the subsolar point at 63 or 92  $R_J$  (Joy et al., 2002). The ionization of neutral material ejected by Io and the subsequent pervasive spread of Iogenic plasma account for the expansive nature of Jupiter's magnetosphere. In the rapidly rotating magnetic field environment, internally produced plasma is transported radially outward (e.g., Bagenal

et al., 2016) and causes the magnetosphere to reach a stretched and bent-back magnetic field configuration (Khurana & Schwarzl, 2005), which leads to the generation of field-aligned currents (FACs) between the ionosphere and magnetosphere. These currents flow radially outward through the magnetosphere and then close back along the magnetic field lines returning through the ionosphere. Lorentz forces act to accelerate the plasma within the magnetosphere toward the corotation velocity (Hill, 1979). Meanwhile, the radial transport of particles in the current sheet leads to small-scale magnetic field perturbations as a result of discontinuous flux tube-driven transport (Mauk & Saur, 2007; Saur et al., 2003; Tao et al., 2015). It is suggested that local deviations in the force or stress balance within Jupiter's magnetosphere-ionosphere coupling prompt these small-scale magnetic field fluctuations to achieve stress balance (Saur et al., 2018). These magnetic field perturbations subsequently cascade to smaller scales as they interact with the magnetic field lines. Locally stressed magnetic field lines generate Alfvén waves, which facilitate momentum transfer between the magnetosphere and the ionosphere. This interaction leads to stochastic acceleration of particles (Saur et al., 2018). The precipitation of energetic particles associated with the corotation enforcement current system (e.g., Cowley & Bunce, 2001; Nichols & Cowley, 2003; Ray et al., 2010; Southwood & Kivelson, 2001), along with particles undergoing stochastic acceleration by Alfvén waves (e.g., Gershman et al., 2019; Kurth et al., 2018; Mauk et al., 2018, 2020; Pan et al., 2021; Salveter et al., 2022; Saur et al., 2018), are thought to contribute significantly to Jupiter's bright main auroral emissions.

Throughout the process, angular momentum transferred from Jupiter to the plasma is facilitated by Alfvén waves (Alfvén, 1942). However, as the plasma's radial distance from Jupiter increases, its radial velocity will incrementally surpass the diminishing Alfvén velocity. This disparity reaches a critical juncture at the Alfvén radius, beyond which the plasma decouples from the ionosphere (Delamere & Bagenal, 2010). Understanding the characteristics of the Alfvén radius is pivotal for comprehending the intricate dynamic interactions within Jupiter's magnetospheric environment, particularly for unraveling the energy and momentum transport processes associated with Jupiter's auroras. Previous studies on the Alfvén radius location within Jupiter's magnetosphere have employed a simplified dipole magnetic field perspective and focused on the equatorial plasma (e.g., Delamere & Bagenal, 2010) because perturbations in the plasma can no longer propagate back toward Jupiter. However, the dipole model is insufficient to account for significant local time (LT) variations in plasma density and the structure of the current disc within Jupiter's magnetosphere (e.g., Cowley & Bunce, 2001; Khurana & Schwarzl, 2005; Krupp et al., 2001; Lorch et al., 2020; Ray et al., 2010). The recent work by Jenkins et al. (2024) marks a significant advancement in this field by integrating these LT asymmetries into their analysis of the Alfvén radius. Their findings reveal an Alfvén radius characterized by a local time-dependent structure, indicating the asymmetric location across different LTs, providing a more accurate picture of the Alfvén radius. Notably, they have identified a minimum Alfvén radius of  $30 R_J$  at midnight and predicted that no Alfvén radius between 8 and 20 LT exists within the  $60 R_J$  boundary of their model. The absence of the Alfvén radius in the noon-to-dusk sectors of the magnetosphere is due to the stronger north-south component of the magnetic field in these sectors (Vogt et al., 2011), which leads to a larger Alfvén velocity relative to the nightside.

This study aims to expand on the work of Jenkins et al. (2024) by using global simulations to examine the location and dynamics of Jupiter's Alfvén radius. Our simulations reveal the dynamic behavior of the Alfvén radius. Additionally, when averaged over one Jovian rotation period, the position of the Alfvén radius displays characteristics remarkably similar to those observed in the static model proposed by Jenkins et al. (2024). These new insights are poised to enhance our understanding of magnetospheric processes within the unique and dynamic magnetic environment of Jupiter.

## 2. Simulation Information

The Grid Agnostic MHD for Extended Research Applications (GAMERA) code, as detailed in Zhang et al. (2019), marks a significant advancement in studying solar wind interactions with outer planetary magnetospheres, furthering the studies for SW-outer planetary magnetosphere interactions (Zhang et al., 2018, 2021). GAMERA utilizes a finite-volume approach to solve ideal MHD equations on a non-orthogonal curvilinear grid specifically adapted for Jupiter's magnetosphere. In the solar-magnetospheric (SM) coordinate system—where the  $X$ ,  $Y$ , and  $Z$  axes align with the Jupiter-Sun direction, eastward (dusk), and north, respectively—the computational framework employs a non-orthogonal stretched spherical grid of  $256 \times 256 \times 128$  cells. This grid, mirroring a spherical (radial  $\times$  meridional  $\times$  azimuthal) coordinate system, increases in resolution with decreasing radial distance from Jupiter, reaching about 0.3 Jovian Radii ( $R_J$ ) near the lower boundary. The model covers a substantial area, extending to  $100 R_J$  toward the Sun,  $-1,000 R_J$  anti-sunward, and  $\pm 300 R_J$  in the

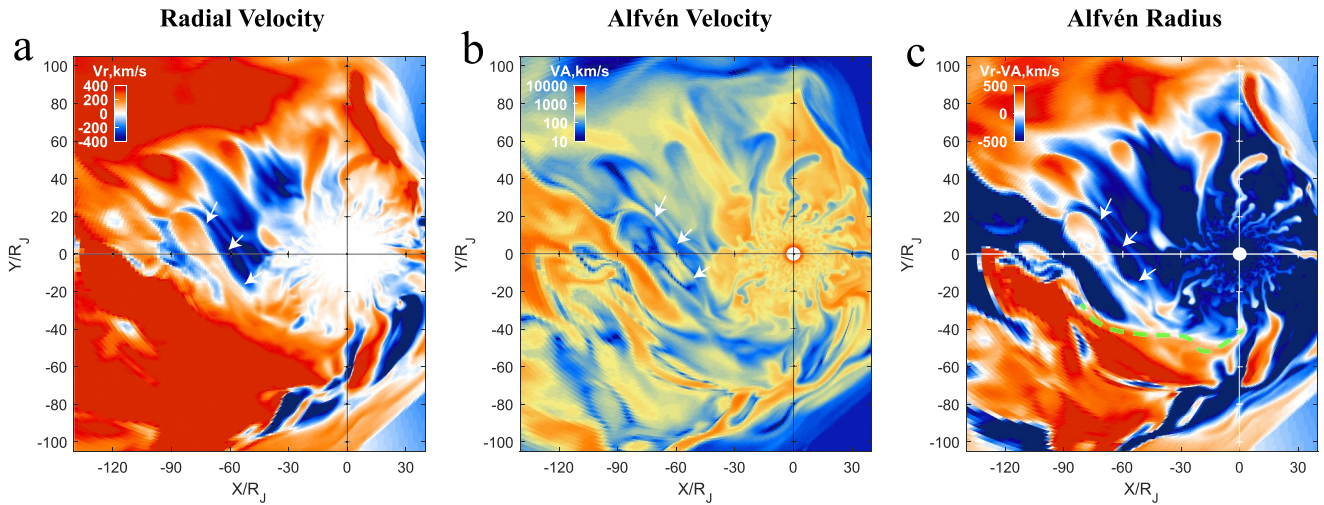


**Figure 1.** Simulation results of (a) plasma radial velocity  $V_r$ , (b) plasma Alfvén velocity  $V_A$ , and (c)  $V_r - V_A$  on the equatorial plane at ST = 319.3 hr. The white regions in (c) indicate where the plasma radial and Alfvén velocities are equal, that is, the location of the Alfvén radius. In (c), the red region in the figures signifies the area where the radial outward velocity of the plasma is dominant. Conversely, the blue region indicates the area where the Alfvén velocity of the plasma dominates. The white arrows show an outward plasma flow potentially associated with plasma loss, where low Alfvén velocities and Alfvén radii are observed. The green dashed line in panel c highlights the region in which the Alfvén radius extends from the post-midnight to the dawn side, outside the reconnection-related Alfvén radius boundary. In addition to this figure, Figures 2 and 5, the dynamic variation can be seen in Movies S1–S3.

perpendicular directions. A spherical volume of radius  $3.5 R_J$ , centered on Jupiter, is excluded from this distorted domain. Simplifying the analysis, the dipole tilt angle is set to zero, eliminating hemispheric asymmetries. Jupiter's 10-hr magnetospheric corotation is simulated by applying a constant corotation potential to the ionospheric potential. The magnetosphere-ionosphere coupling is modeled using the electrostatic current closure method, which involves solving a Poisson equation at the ionospheric reference altitude. This method primarily accounts for the effects of solar wind-magnetosphere (SW-M) coupling. A corotation potential is imposed as a boundary condition in conjunction with the SW-M potential (Feng et al., 2023; Zhang et al., 2019, 2021). The model also incorporates ion mass loading from the Io plasma torus using a spatial function (Feng et al., 2023) with a fixed Io mass loading rate of approximately  $1,000 \text{ kg s}^{-1}$ , centered at  $6 R_J$  in the equatorial plane. Reflecting typical solar wind conditions (Blanc et al., 2005; Delamere & Bagenal, 2010), the upstream IMF  $B_y$ , solar wind density, and velocity are set at  $0.5 \text{ nT}$ ,  $0.25 \text{ cm}^{-3}$ , and  $350 \text{ km s}^{-1}$ , respectively.

### 3. Simulation Results

Figure 1 shows the snapshot from the simulation at ST = 319.3 hr displaying the instantaneous locations of magnetospheric plasma radial velocity  $V_r$ , the Alfvén velocity  $V_A$  and the difference between  $V_r$  and  $V_A$  ( $V_r - V_A$ ) in the equatorial plane.  $V_A$  is calculated by

$$V_A = \frac{B}{\sqrt{\mu_0 \rho}} \quad (1)$$

where  $\rho$  is the plasma mass density. It is noted that this simulation uses a single-component model comprised of protons. The mass density is calculated by multiplying the proton number density by the proton mass.  $B$  is the magnitude of the magnetic field and  $\mu_0$  is vacuum magnetic permeability. Figure 1 illustrates the simulated complex spatial variation of Jupiter's radial velocity, Alfvén velocity, and Alfvén radius within its intricate rotating magnetospheric environment. Large interchange structures can be identified in Figures 1a and 1b. For example, an outward ( $V_r > 0$ ) plasma flow extends all the way from  $\sim 90 R_J$  pre-midnight to  $\sim 40 R_J$  as the arrows in Figure 1a indicate. A strong inward plasma flow (blue regions) is displayed in the inner boundary of the outward flow region, which may be associated with plasma loss attributable to the Vasyliūnas Cycle in the nightside magnetosphere and the accompanying magnetic reconnection process (Louarn et al., 2015; Vasyliūnas, 1983; Vogt et al., 2010). Around the inner edge of this feature, Alfvén velocities are observed to be low, as indicated by the arrows in Figure 1b. Moreover, the plasma radial outward velocity in this region closely

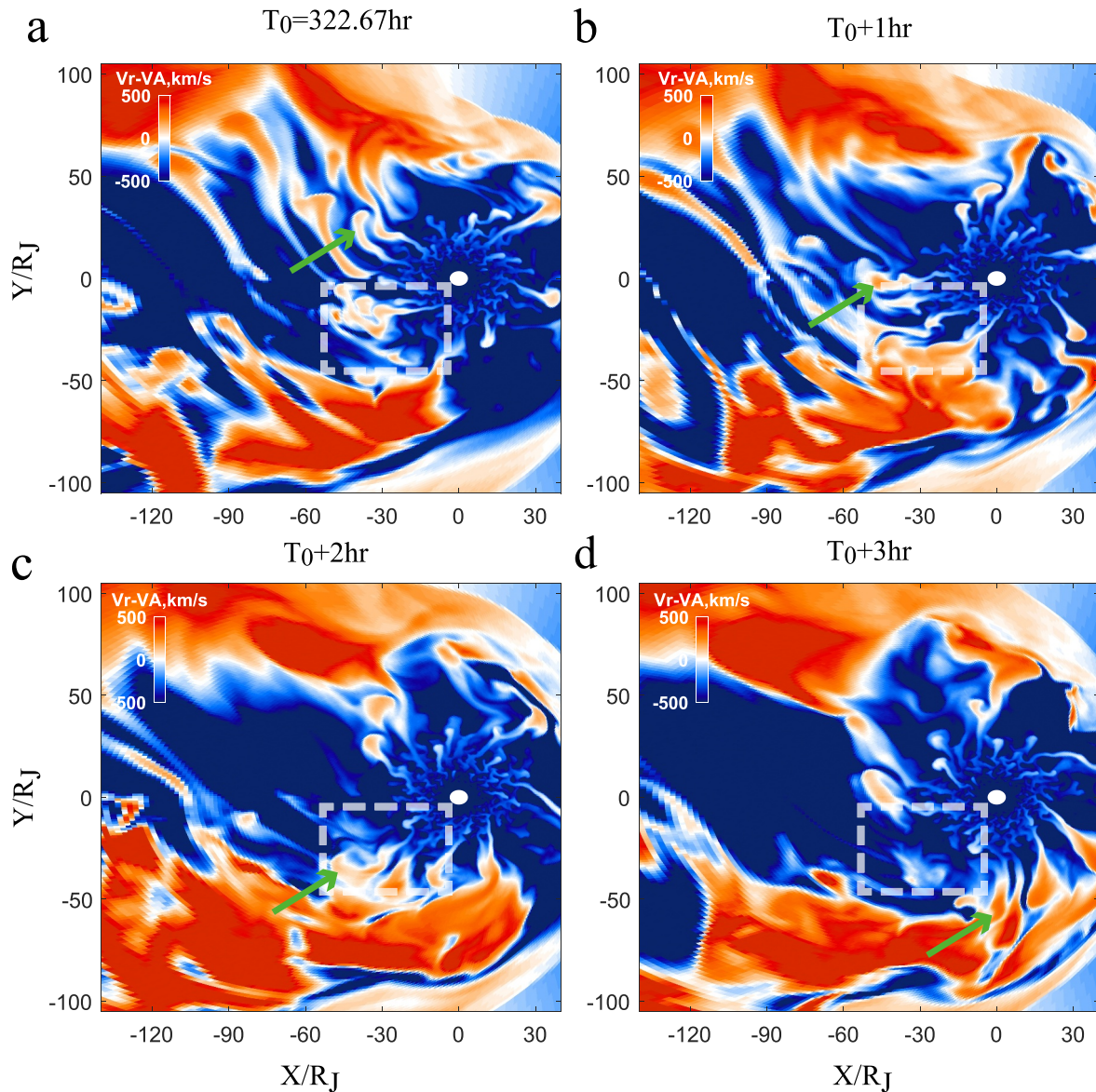


**Figure 2.** Alfvén radius variations on the equatorial plane at four different times: (a)  $ST = t_0 = 322.67$  hr; (b)  $t_0 + 1$  h; (c)  $t_0 + 2$  h; (d)  $t_0 + 3$  h. The dashed box region, consistently labeled in each snapshot, serves as a reference for comparing the variations of Alfvén radii across the snapshots. The green arrows in panels (a–d) point to the same Alfvén radius structure during rotations.

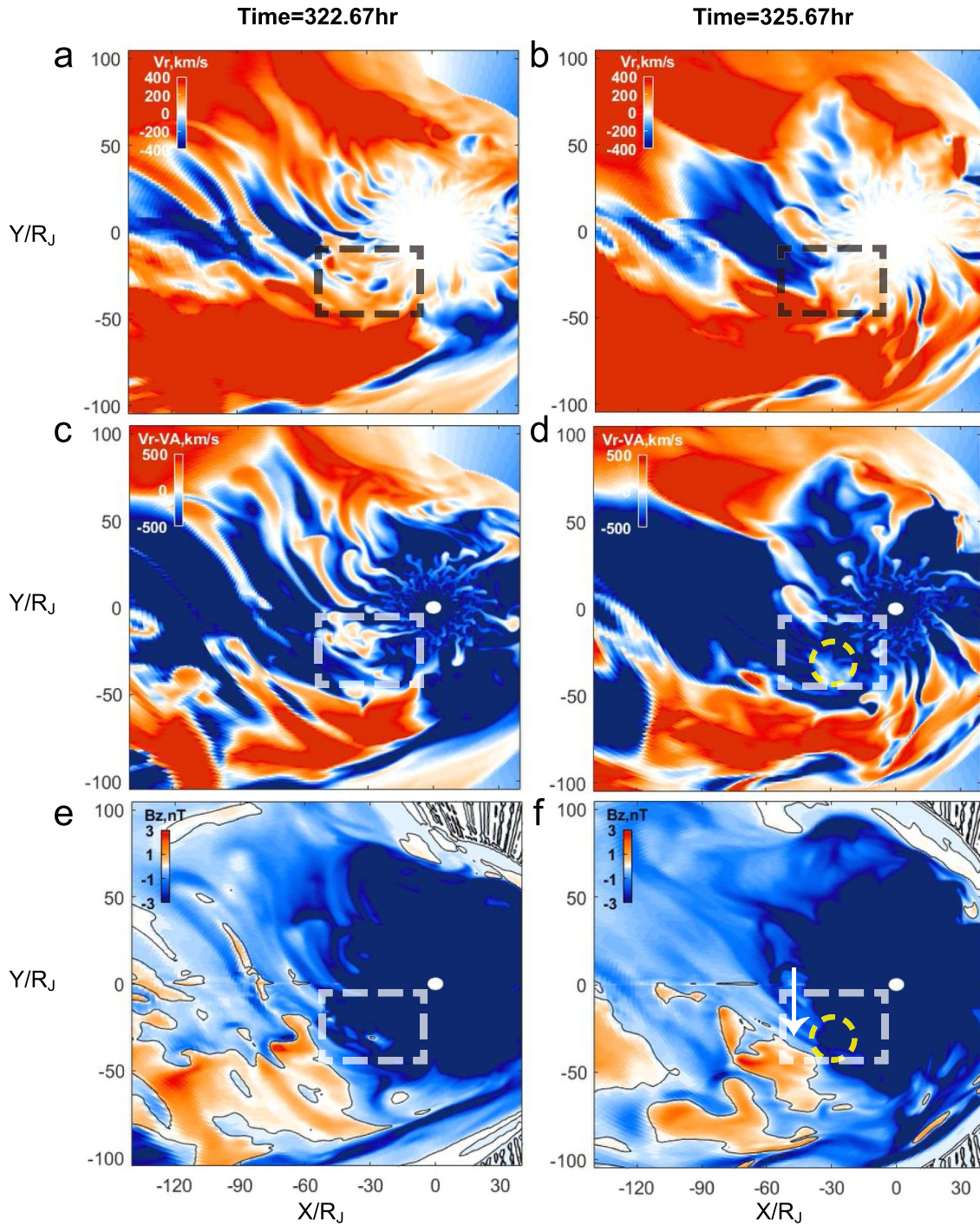
approximates the Alfvén velocities, resulting in the identification of the Alfvén radius in this sector, which is shown by the white regions in Figure 1c. The green dashed line in Figure 1c highlights the extension of the Alfvén radius from post-midnight to the dawn side, located outside the potential reconnection-related Alfvén radius boundary. This region is characterized by radially outward-transported plasma velocities surpassing Alfvén velocities, constituting the primary region of interest in this study. In summary, Figure 1c unveils complex multilayer structures of the Alfvén radius, ranging from proximal to distant regions, which are interspersed with sporadic small-scale formations most likely linked with the interchange instability phenomenon. The sharp plasma density cavity characteristics and abrupt magnetic field changes, which are the typical features of the interchange instability, are displayed at the Alfvén radius in Figures S3–S5 of Supporting Information S1.

Figure 2 shows four snapshots at intervals of 1 hr each, displaying the locations and structures of Jupiter's Alfvén radius on the equatorial plane as obtained from the simulation. These snapshots reveal dynamic variations and rotational modulations of the Alfvén radius over a 3-hr interval. By tracking the same Alfvén radius structure,

clear rotational modulation could be observed by its noticeable LT changes, as indicated by the green arrows in Figures 2a–2d. Furthermore, when focusing on a fixed sector, the Alfvén radius features appear and disappear over time. We constructed a box region between the midnight and dawn side near  $50 R_J$  (marked with white dashed boxes in Figure 2) to focus on the most notable variations, and the Alfvén radius in this region is evidently unstable spanning across these 3 hr. Specifically, the significant variations in Alfvén radius presence in the box region (Figures 2a–2c) suggest an effective transient decoupling between the magnetosphere and planet in this region. Conversely, the Alfvén radius structure previously formed has diminished in the box region after 1 hr (Figure 2d), likely corotating azimuthally to the dayside, suggesting a rapid re-coupling of the magnetosphere and ionosphere in the box region. The green arrows in Figures 2a–2d point to the same Alfvén radius structure corotating throughout the simulation (see Movie S2), which further suggests that the temporal variation of the Alfvén radius is influenced by Jupiter's rotation. It should be noted that temporal and spatial variations of the Alfvén radius, strongly modulated by the planet's rotation, are observable at all local times. This result indicates the dynamic variability of the coupling states between the magnetosphere and Jupiter throughout the entire system.

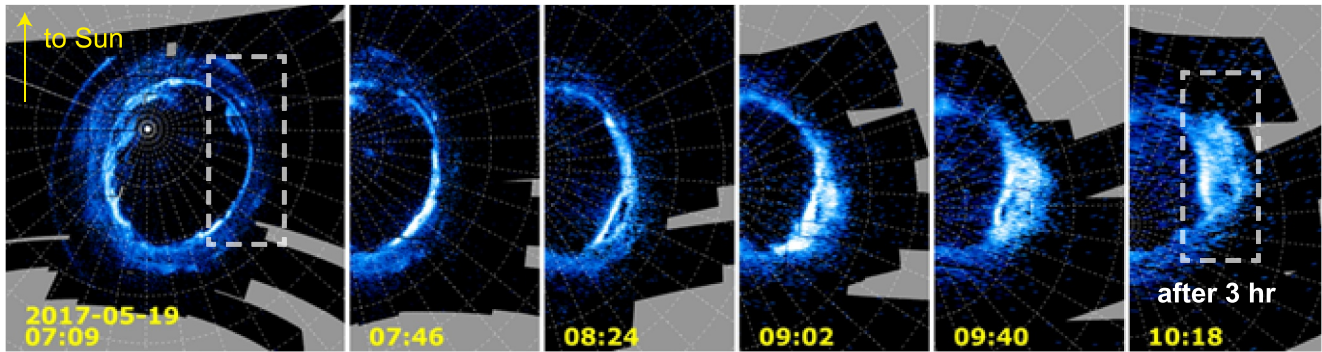
Figure 3 presents a detailed comparison of simulation results for the intervals  $ST = 322.67$  and  $ST = 325.67$  hr, corresponding to Figures 2a and 2d, respectively. The comparison figure displays significant variability in the Alfvén radius location, plasma radial velocity, and X-line in the dawnside boxed region before and after 3 hr (Figures S1–S2 in Supporting Information S1 show more detailed information of the two moments). In Figure 3e, the X-line of the magnetotail reconnection on the post-midnight side is positioned on the outer side of the region highlighted in the box. By  $ST = 325.67$  hr, as shown in Figure 3f, the X-line has moved inward but remains radially outside of the weak Alfvén radius. Figure 4 displays the evolution of a dawn storm in Jupiter's polar auroras from a quiet to enhanced state on a  $\sim 3$ -hr timescale. The illuminated region is constantly changing and evolving and could roughly map to  $10$ – $40 R_J$  in the magnetosphere (Bonfond et al., 2021; Connerney et al., 2018; Vogt et al., 2015). The observable contrast between the quiet aurora at 19th May 2017 07:09 and its intensification at 10:18 ( $\sim 3$  hr after) reflects distinct states in the magnetosphere, which are potentially associated with the processes of decoupling and recoupling shown in Figure 3. At  $T_0 = 322.67$  hr, depicted in Figure 2a, magnetotail reconnection takes place outside the Alfvén radius ( $\sim 60 R_J$ , refer to Figure 3e). The boxed region inside the X-line is dominated by the radial outward flows shown in Figure 3a, which displays that the reconnection inward flow didn't move in effectively. Concurrently, Jupiter's inner magnetosphere remains undisturbed by reconnection-driven flows, potentially correlating with a quiet auroral display (as depicted in the left panel of Figure 4). Over time, planetward high-velocity flows initiated by post-midnight reconnection would lead to a buildup of magnetic pressure. This process causes the radial outward plasma velocity  $V_r$  to decrease, while the accumulation of magnetic flux strengthens the magnetic field and increases the Alfvén velocity  $V_A$ . Consequently, the differential value of  $V_r - V_A$  diminishes to a negative figure, resulting in the gradual disappearance of the Alfvén radius, as displayed in Figure 3d. At this stage, the reconnected high-speed flow can be efficiently transported toward the planets, as depicted in Figure 3b. The continuous compression caused by planetward high-speed flow fosters a buildup of magnetic energy and induces perturbations in the near-Jupiter magnetotail, yielding two significant outcomes: a. The accumulation of magnetic energy disrupts the current system and leads to the formation of FACs, enhancing the auroral activity (Birn et al., 2004; Li et al., 2011; Yao et al., 2012, 2013); b. Perturbations in the mid- and near-magnetic tails generate Alfvén waves, contributing to auroral brightening (Gershman et al., 2019; Salveter et al., 2022; Saur et al., 2018). In summary, the transition from quiet to enhanced auroral activity around the 3 hrs may be associated with the decoupling and recoupling processes that are represented by the changing azimuthal location of the post-midnight Alfvén radius, which is driven by the competing inward reconnection-driven flow and bulk outflow during this period.

Figure 5 presents the 10-hr averaged simulation results of plasma radial velocity, Alfvén velocity, and Alfvén radius. As shown in Figure 5a, after averaging over one rotation period (from  $ST = 324.50$  to  $334.50$  hr), the region with dominant radial outward transport of plasma is primarily located on the afternoon (roughly 11–19 LT) and dawn (roughly 2–7 LT) sides. Conversely, the radial inward transport region is concentrated around midnight (roughly 19–2 LT) and pre-noon (roughly 7–11 LT), with the magnitude of radial velocity increasing with radial distance. Figure 5b displays the averaged picture of Alfvén velocity, highlighting extended strips of decreasing velocity between approximately  $30$  and  $60 R_J$  from the night side to the dawn side. This decreasing pattern of the Alfvén velocity resembles the Alfvén velocity distribution proposed by Jenkins et al. (2024) in their static model. Over different 10-hr periods, there is almost no significant change in the average Alfvén velocity picture.



**Figure 3.** (a, c, e) Radial velocity, Alfvén radius location, and  $B_z$  at time 322.67 hr, corresponding to Figure 2a, (b, d, f) radial velocity, Alfvén radius location, and  $B_z$  at time 325.67 hr, corresponding to Figure 2d. Since the dipole tilt angle is set to zero in the simulation, the variation of  $B_z$  from negative to positive is instrumental in identifying the magnetic reconnections (x-line) within the magnetotail. The dashed box regions serve as a reference for comparing the variations of Alfvén radii, plasma radial velocity and x-line, corresponding to Figure 2. The yellow circle in panel f highlights the location of the disappearing Alfvén radius, corresponding to panel d, which is situated inside the x-line. The white arrow indicates that the x-line has shifted inward at ST = 325.67 hr compared to its position at ST = 322.67 hr.

Figure 5c shows the averaged picture of the Alfvén radius. We mainly focus on the white boundary region where the radial velocity of the plasma first surpasses the Alfvén velocity, which is indicated by the white dashed line in the figures. After 10 hr of averaging, the initially complex transient structure of the Alfvén radius stabilizes,



**Figure 4.** The sequence of images shows the  $\sim 3$ -hr evolution of a dawn storm in Jupiter's polar auroras, from left to right. These observations come from Juno's UVS (Ultraviolet Spectrograph) instrument data adapted from Bonfond et al. (2021). Source: NASA/JPL-Caltech/SwRI/UVS/ULiège/Bonfond.

revealing an asymmetric pattern extending from the night side to the morning side. This asymmetry, focused from the midnight side to the morning side, aligns closely with the distribution reported in Jenkins et al. (2024)'s static model, which is a noteworthy finding.

Over various 10-hr periods, while there are no significant overall changes in averaged plasma radial velocity distribution, its variations in specific regions can be observed, as shown in Movie S3. For example, in the far magnetic tail region ( $\sim 90 R_J$ ,  $\sim 3$  LT), there is a noticeable evolution of the average radial velocity from an outward direction to an inward direction. This shift significantly influences the Alfvén radius feature in the same region, leading to a reduced influence of the red region dominated by radial velocity before dawn, as shown in Figure 5c. The outer boundary of this region also moves toward Jupiter. But notably, the inner structure of the Alfvén radius, delineated by the white dashed line in Figure 5c, remains relatively stable, as depicted in Movie S3. This persistent feature is in stark contrast to the dynamic temporal variations of the Alfvén radius observed in Figure 2. However, there is an outward shift toward the dawnside magnetopause in the dynamic model: the maximum distance of the Alfvén radius in the static model is around  $30 R_J$ , while it reaches  $60 R_J$  in our simulation. This disparity might stem from the idealized conditions assumed in the static model, such as a uniform radial velocity of plasma across the same radial distance, or assuming a proton plasma rather than heavier constituents, as considered by Jenkins et al. (2024). In contrast, the simulation reflects more dynamic conditions. Variations in the simulation parameters, such as mass loading and solar wind conditions, could also account for the differing Alfvén radius features. Movies S4 and S5 display the averaged  $V_r$ ,  $V_A$ , and  $V_r - V_A$  simulation results averaged over periods of 20 and 40 hr, respectively. As the duration of the averaging period increases, the variability in the average picture decreases, with features being more consistent.

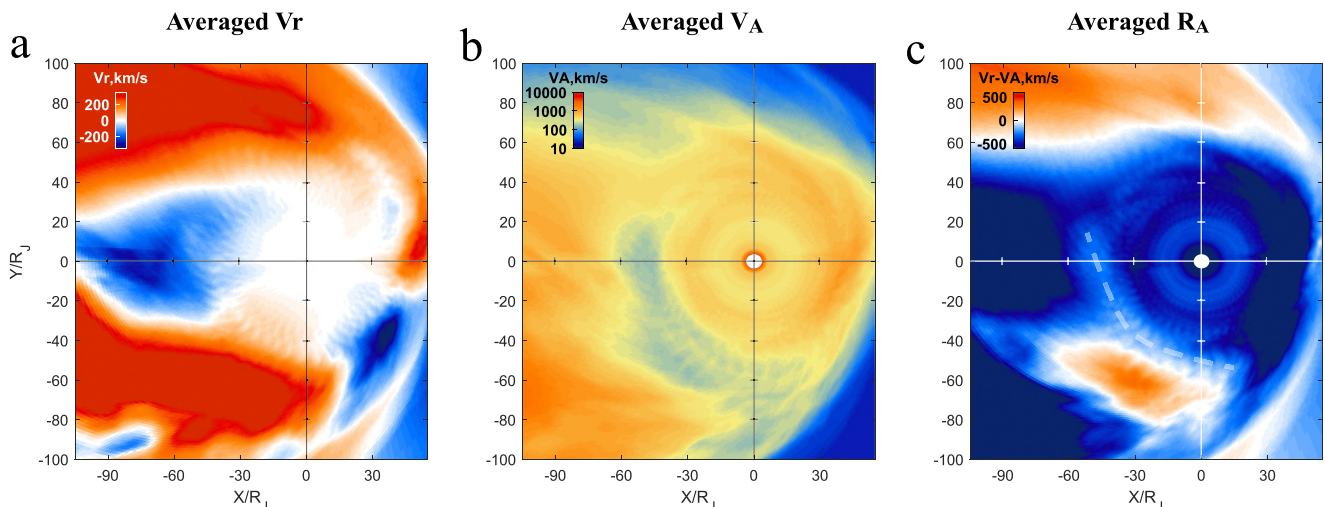


**Figure 5.** The averaged simulation results of (a)  $V_r$  (b)  $V_A$ , and (c)  $V_r - V_A$  on the equatorial plane. All are averaged over one Jupiter rotation period (10 hr) from ST = 324.50 to ST = 334.50 hr. The white dashed line in panel c shows the location of the averaged Alfvén radii inner boundary.

#### 4. Conclusion

This research, utilizing high-resolution simulations, delves into the Alfvén radius within Jupiter's magnetosphere, unveiling its dynamic characteristics. Our results extend the perspective of the static model by demonstrating significant dynamic variations in the Alfvén radius, which are strongly influenced by the rotating magnetosphere. These variations illuminate the complex interaction between Jupiter's magnetic field and the surrounding plasma, which is affected by various factors such as internal plasma dynamics and solar wind interactions. The dynamic evolution of Jupiter's Alfvén radius and reconnection sites reveals complex behaviors of magnetospheric-planetary coupling and decoupling at varying local times and radial distances. The “small-scale” Alfvén radius structures observed at various local times are likely associated with interchange instability structures (as shown in Figures S3–S5 of Supporting Information S1). Centrifugal interchange of the flux tube occurs actively in radial directions, producing small-scale radial outward and inward moving structures, as shown in Figure 1a. When the radial outward velocity of the structure surpasses the Alfvén velocity, it would significantly impede the radial transmission of Alfvénic communication in the region, leading to decoupling from the ionosphere. The decoupling and recoupling processes alternate with corotation. This variation of Alfvén radius structures could intricately link to the observed complex auroral-enhanced regions which dynamically change (Bonfond et al., 2021; Greathouse et al., 2021; Yao et al., 2020).

Crucially, it can be concluded from our study that the average location of the Alfvén radius over one Jupiter rotation period aligns with Jenkins et al. (2024)'s static model. This resemblance is seen in the bulge-shaped boundary facing  $\sim 03$  LT, and a notable absence of the Alfvén radius between the post-dawn and dusk sectors. The observed asymmetry in the Alfvén radius location underscores the inherent non-uniformities in plasma distribution and magnetic field strength across different sectors of Jupiter's magnetosphere, which could correspond to the observed strong local time control within the polar collar (Greathouse et al., 2021; Grodent et al., 2003). The finding that our simulation is in alignment with the static models on the average picture of Alfvén radius and the local time asymmetry suggests that, despite the presence of transient dynamic processes and phenomena, there is an underlying pattern influenced by Jupiter's rotational dynamics and the solar wind's interaction with the magnetosphere. This persistent pattern, evident in the averaged data, will be key to advancing our understanding of the behaviors of giant planetary magnetospheres and the energy transportation processes related to auroral illumination.

Furthermore, corresponding to a class of auroral enhancement events closely linked to solar wind compression (e.g., Grodent et al., 2018; Xu et al., 2023; Yao et al., 2022), it is worth examining the evolutionary properties of the Alfvén radius under various solar wind conditions in a future study. Future research should delve deeper into the coupling processes and further elucidate the impact of solar wind compression on the dynamic behavior of Jupiter's magnetosphere.

#### Data Availability Statement

The model outputs used to generate the figures for the analysis presented in this paper are publicly available online (Xu, 2024).

#### Acknowledgments

Z. Y. acknowledges the National Natural Science Foundation of China (Grants 42074211 and 42374212). BZ is supported by the Excellent Young Scientists Fund (Hong Kong and Macau) of the National Natural Science Foundation of China (Grant 41922060), the General Program of the National Natural Science Foundation of China (Grant 42374216) and the Research Grants Council (RGC) General Research Fund (Grants 17308221, 17308520, 17315222, and 17308723). SVB was supported by STFC Grants ST/V000748/1 and ST/Y002393/1. B. Bonfond is a Research Associate of the Fonds de la Recherche Scientifique—FNRS.

#### References

- Alfvén, H. (1942). Existence of electromagnetic-hydrodynamic waves. *Nature*, *150*(3805), 405–406. <https://doi.org/10.1038/150405d0>
- Bagenal, F., Wilson, R. J., Siler, S., Paterson, W. R., & Kurth, W. S. (2016). Survey of Galileo plasma observations in Jupiter's plasma sheet. *Journal of Geophysical Research*, *121*(5), 871–894. <https://doi.org/10.1002/2016je005009>
- Birn, J., Raeder, J., Wang, Y. L., Wolf, R. A., & Hesse, M. (2004). On the propagation of bubbles in the geomagnetic tail. In *Annales geophysicae*, (Vol. 22(5), pp. 1773–1786). Göttingen, Germany: Copernicus Publications. <https://doi.org/10.5194/angeo-22-1773-2004>
- Blanc, M., Kallenbach, R., & Erkaev, N. V. (2005). Solar system magnetospheres. *Space Science Reviews*, *116*(1–2), 227–298. [https://doi.org/10.1007/1-4020-4038-5\\_15](https://doi.org/10.1007/1-4020-4038-5_15)
- Bonfond, B., Yao, Z. H., Gladstone, G. R., Grodent, D., Gérard, J. C., Matar, J., et al. (2021). Are dawn storms Jupiter's Auroral substorms? *AGU Advances*, *2*(1), e2020AV000275. <https://doi.org/10.1029/2020av000275>
- Connerney, J. E. P., Kotsiaros, S., Oliverson, R. J., Espley, J. R., Joergensen, J. L., Joergensen, P. S., et al. (2018). A new model of Jupiter's magnetic field from Juno's first Nine Orbits. *Geophysical Research Letters*, *45*(6), 2590–2596. <https://doi.org/10.1002/2018gl077312>
- Cowley, S. W. H., & Bunce, E. J. (2001). Origin of the main Auroral oval in Jupiter's coupled magnetosphere-ionosphere system. *Planetary and Space Science*, *49*(10–11), 1067–1088. [https://doi.org/10.1016/s0032-0633\(00\)00167-7](https://doi.org/10.1016/s0032-0633(00)00167-7)
- Delamere, P. A., & Bagenal, F. (2010). Solar wind interaction with Jupiter's magnetosphere. *Journal of Geophysical Research*, *115*(A10), 10170–10199. <https://doi.org/10.1029/2010ja015347>



- Feng, E., Zhang, B., Yao, Z., Delamere, P. A., Zheng, Z., Dunn, W. R., & Ye, S.-Y. (2023). Variation of the Jovian magnetopause under constant solar wind conditions: Significance of magnetodisc dynamics. *Geophysical Research Letters*, *50*(12), e2023GL104046. <https://doi.org/10.1029/2023GL104046>
- Gershman, D. J., Connerney, J. E. P., Kotsiaros, S., DiBraccio, G. A., Martos, Y. M., Viñas, A. F., et al. (2019). Alfvénic fluctuations associated with Jupiter's Auroral emissions. *Geophysical Research Letters*, *46*(13), 7157–7165. <https://doi.org/10.1029/2019gl082951>
- Greathouse, T., Gladstone, R., Versteeg, M., Hue, V., Kammer, J., Giles, R., et al. (2021). Local time dependence of Jupiter's polar auroral emissions observed by Juno UVS. *Journal of Geophysical Research: Planets*, *126*(12), e2021JE006954. <https://doi.org/10.1029/2021je006954>
- Grodent, D., Bonfond, B., Yao, Z., Gérard, J.-C., Radioti, A., Dumont, M., et al. (2018). Jupiter's aurora observed with HST during Juno Orbits 3 to 7. *Journal of Geophysical Research*, *123*(5), 3299–3319. <https://doi.org/10.1002/2017ja025046>
- Grodent, D., Clarke, J. T., Waite, J. H., Cowley, S. W. H., Gérard, J.-C., & Kim, J. (2003). Jupiter's polar Auroral emissions. *Journal of Geophysical Research*, *108*(A10), e2021JE006954. <https://doi.org/10.1029/2003ja010017>
- Hill, T. W. (1979). Inertial limit on corotation. *Journal of Geophysical Research*, *84*(A11), 6554–6558. <https://doi.org/10.1029/ja084ia11p06554>
- Hill, T. W., Dessler, A. J., & Goertz, C. K. (1983). Magnetospheric models.
- Jenkins, A., Ray, L. C., Fell, T., Badman, S. V., & Lorch, C. T. S. (2024). Revealing the local time structure of Alfvén Radii and travel times in the Jovian magnetosphere. *Journal of Geophysical Research*. <https://doi.org/10.17635/lancaster/researchdata/661>
- Joy, S. P., Kivelson, M. G., Walker, R. J., Khurana, K. K., Russell, C. T., & Ogino, T. (2002). Probabilistic models of the Jovian magnetopause and bow shock locations. *Journal of Geophysical Research*, *107*(A10), 1309. <https://doi.org/10.1029/2001ja009146>
- Khurana, K. K., & Schwarzl, H. K. (2005). Global structure of Jupiter's magnetospheric current sheet. *Journal of Geophysical Research*, *110*(A7), A07227. <https://doi.org/10.1029/2004ja010757>
- Krupp, N., Woch, J., Lagg, A., Roelof, E. C., Williams, D. J., Livi, S., & Wilken, B. (2001). Local time asymmetry of energetic ion anisotropies in the Jovian magnetosphere. *Planetary and Space Science*, *49*(3–4), 283–289. [https://doi.org/10.1016/s0032-0633\(00\)00149-5](https://doi.org/10.1016/s0032-0633(00)00149-5)
- Kurth, W. S., Mauk, B. H., Elliott, S. S., Gurnett, D. A., Hospodarsky, G. B., Santolík, O., et al. (2018). Whistler mode waves associated with broadband Auroral electron precipitation at Jupiter. *Geophysical Research Letters*, *45*(18), 9372–9379. <https://doi.org/10.1029/2018gl078566>
- Li, S. S., Angelopoulos, V., Runov, A., Zhou, X. Z., McFadden, J., Larson, D., et al. (2011). On the force balance around dipolarization fronts within Bursty bulk flows. *Journal of Geophysical Research*, *116*(A5), A00135. <https://doi.org/10.1029/2010ja015884>
- Lorch, C. T. S., Ray, L. C., Arridge, C. S., Khurana, K. K., Martin, C. J., & Bader, A. (2020). Local time asymmetries in Jupiter's magnetodisc currents. *Journal of Geophysical Research: Space Physics*, *125*(2), e2019JA027455. <https://doi.org/10.1029/2019ja027455>
- Louam, P., Andre, N., Jackman, C. M., Kasahara, S., Kronberg, E. A., & Vogt, M. F. (2015). Magnetic reconnection and associated transient phenomena within the magnetospheres of Jupiter and Saturn. *Space Science Reviews*, *187*, 181–227. [https://doi.org/10.1007/978-1-4939-3395-2\\_6](https://doi.org/10.1007/978-1-4939-3395-2_6)
- Mauk, B. H., Clark, G., Gladstone, G. R., Kotsiaros, S., Adriani, A., Allegrini, F., et al. (2020). Energetic particles and acceleration regions over Jupiter's polar cap and main aurora: A broad overview. *Journal of Geophysical Research*, *125*(3), e2019JA027699. <https://doi.org/10.1029/2019ja027699>
- Mauk, B. H., Haggerty, D. K., Paranicas, C., Clark, G., Kollmann, P., Rymer, A. M., et al. (2018). Diverse electron and ion acceleration characteristics observed over Jupiter's main aurora. *Geophysical Research Letters*, *45*(3), 1277–1285. <https://doi.org/10.1002/2017gl076901>
- Mauk, B. H., & Saur, J. (2007). Equatorial electron beams and auroral structuring at Jupiter. *Journal of Geophysical Research*, *112*(A10), A10221. <https://doi.org/10.1029/2007ja012370>
- Nichols, J. D., & Cowley, S. W. H. (2003). Magnetosphere-ionosphere coupling currents in Jupiter's middle magnetosphere: Dependence on the effective Ionospheric Pedersen conductivity and Iogenic plasma mass outflow rate. *Annales Geophysicae*, *21*(7), 1419–1441. <https://doi.org/10.5194/angeo-21-1419-2003>
- Pan, D. X., Yao, Z. H., Manners, H., Dunn, W., Bonfond, B., Grodent, D., et al. (2021). Ultralow-frequency waves in driving Jovian aurorae revealed by observations from HST and Juno. *Geophysical Research Letters*, *48*(5), e2020GL091579. <https://doi.org/10.1029/2020gl091579>
- Ray, L. C., Ergun, R. E., Delamere, P. A., & Bagenal, F. (2010). Magnetosphere-ionosphere coupling at Jupiter: Effect of field-aligned potentials on angular momentum transport. *Journal of Geophysical Research*, *115*(A9), A09211. <https://doi.org/10.1029/2010ja015423>
- Salveter, A., Saur, J., Clark, G., & Mauk, B. H. (2022). Jovian auroral electron precipitation budget—A statistical analysis of diffuse, Monoenergetic, and broadband auroral electron distributions. *Journal of Geophysical Research*, *127*(8), e2021JA030224. <https://doi.org/10.1029/2021ja030224>
- Saur, J., Janser, S., Schreiner, A., Clark, G., Mauk, B. H., Kollmann, P., et al. (2018). Wave-particle interaction of Alfvén waves in Jupiter's magnetosphere: Auroral and magnetospheric particle acceleration. *Journal of Geophysical Research*, *123*(11), 9560–9573. <https://doi.org/10.1029/2018ja025948>
- Saur, J., Pouquet, A., & Matthaeus, W. H. (2003). An acceleration mechanism for the generation of the main auroral oval on Jupiter. *Geophysical Research Letters*, *30*(5), 1260. <https://doi.org/10.1029/2002gl015761>
- Southwood, D. J., & Kivelson, M. G. (2001). A new perspective concerning the influence of the solar wind on the Jovian magnetosphere. *Journal of Geophysical Research*, *106*(A4), 6123–6130. <https://doi.org/10.1029/2000ja000236>
- Tao, C., Kimura, T., Badman, S. V., André, N., Tsuchiya, F., Murakami, G., et al. (2015). Variation of Jupiter's aurora observed by Hisaki/exceed: 2. Estimations of auroral parameters and magnetospheric dynamics. *Journal of Geophysical Research*, *121*(5), 4055–4071. <https://doi.org/10.1002/2015ja021272>
- Vasyliūnas, V. M. (1983). Plasma distribution and flow. *Physics of the Jovian magnetosphere*, *1*, 395–453. <https://doi.org/10.1017/cbo9780511564574.013>
- Vogt, M. F., Bunce, E. J., Kivelson, M. G., Khurana, K. K., Walker, R. J., Radioti, A., et al. (2015). Magnetosphere-ionosphere mapping at Jupiter: Quantifying the effects of using different internal field models. *Journal of Geophysical Research*, *120*(4), 2584–2599. <https://doi.org/10.1002/2014ja020729>
- Vogt, M. F., Kivelson, M. G., Khurana, K. K., Joy, S. P., & Walker, R. J. (2010). Reconnection and flows in the Jovian magnetotail as inferred from magnetometer observations. *Journal of Geophysical Research*, *115*(A6). <https://doi.org/10.1029/2009ja015098>
- Vogt, M. F., Kivelson, M. G., Khurana, K. K., Walker, R. J., Bonfond, B., Grodent, D., & Radioti, A. (2011). Improved mapping of Jupiter's auroral features to magnetospheric sources. *Journal of Geophysical Research*, *116*(A3), A03220. <https://doi.org/10.1029/2010ja016148>
- Xu, Y. (2024). Alfvén radius simulation data [Dataset]. *OSF*. <https://doi.org/10.17605/OSF.IO/CEXGH>
- Xu, Y., Yao, Z. H., Zhang, B., Delamere, P. A., Ray, L. C., Dunn, W. R., et al. (2023). On the relation between Jupiter's aurora and the dawnside current sheet. *Geophysical Research Letters*, *50*(13), e2023GL104123. <https://doi.org/10.1029/2023gl104123>
- Yao, Z., Sun, W. J., Fu, S. Y., Pu, Z. Y., Liu, J., Angelopoulos, V., et al. (2013). Current structures associated with dipolarization fronts. *Journal of Geophysical Research*, *118*(11), 6980–6985. <https://doi.org/10.1002/2013ja019290>

- Yao, Z. H., Bonfond, B., Clark, G., Grodent, D., Dunn, W. R., Vogt, M. F., et al. (2020). Reconnection-and dipolarization-driven auroral dawn storms and injections. *Journal of Geophysical Research: Space Physics*, *125*(8), e2019JA027663. <https://doi.org/10.1029/2019ja027663>
- Yao, Z. H., Bonfond, B., Grodent, D., Chané, E., Dunn, W. R., Kurth, W. S., et al. (2022). On the relation between auroral Morphologies and compression conditions of Jupiter's magnetopause: Observations from Juno and the Hubble space telescope. *Journal of Geophysical Research*, *127*(10), e2021JA029894. <https://doi.org/10.1029/2021ja029894>
- Yao, Z. H., Pu, Z. Y., Fu, S. Y., Angelopoulos, V., Kubyshkina, M., Xing, X., et al. (2012). Mechanism of substorm current wedge formation: THEMIS observations. *Geophysical Research Letters*, *39*(13), L13102. <https://doi.org/10.1029/2012gl052055>
- Zhang, B., Delamere, P. A., Ma, X., Burkholder, B., Wiltberger, M., Lyon, J. G., et al. (2018). Asymmetric Kelvin-Helmholtz instability at Jupiter's magnetopause boundary: Implications for corotation-dominated systems. *Geophysical Research Letters*, *45*(1), 56–63. <https://doi.org/10.1002/2017gl076315>
- Zhang, B., Delamere, P. A., Yao, Z., Bonfond, B., Lin, D., Sorathia, K. A., et al. (2021). How Jupiter's unusual magnetospheric topology structures its aurora. *Science Advances*, *7*(15), eabd1204. <https://doi.org/10.1126/sciadv.abd1204>
- Zhang, B., Sorathia, K. A., Lyon, J. G., Merkin, V. G., Garretson, J. S., & Wiltberger, M. (2019). GAMERA: A three-dimensional finite-volume MHD solver for non-orthogonal curvilinear geometries. *The Astrophysical Journal - Supplement Series*, *244*(1), 20. <https://doi.org/10.3847/1538-4365/ab3a4c>